Adv. Composite Mater., Vol. 16, No. 2, pp. 115–134 (2007)

Also available online - www.brill.nl/acm

Numerical study for identifying damage in open-hole composites with embedded FBG sensors and its application to experiment results

S. YASHIRO [1,*], K. MURAI [2], T. OKABE [3] and N. TAKEDA [4]

[1] *Graduate School of Science and Engineering, Ehime University, 3 Bunkyo-cho, Matsuyama, Ehime 790-8577, Japan*
[2] *Keio University, 3-14-1 Hiyoshi, Kohoku-ku, Yokohama 223-8522, Japan (Currently: Pipeline Technology Center, Tokyo Gas Co., Ltd.)*
[3] *Department of Aerospace Engineering, Tohoku University, 6-6-01 Aoba-yama, Aoba-ku, Sendai 980-8579, Japan*
[4] *Department of Advanced Energy, Graduate School of Frontier Sciences, The University of Tokyo, 5-1-5 Kashiwanoha, Kashiwa, Chiba 277-8561, Japan*

Received 28 June 2006; accepted 26 July 2006

Abstract—This study proposes two new approaches for identifying damage patterns in a holed CFRP cross-ply laminate using an embedded fiber Bragg grating (FBG) sensor. It was experimentally confirmed that the reflection spectrum from the embedded FBG sensor was significantly deformed as the damage near the hole (i.e. splits, transverse cracks and delamination) extended. The damage patterns were predicted using forward analysis (a damage analysis and an optical analysis) with strain estimation and the proposed damage-identification method as well as the forward analysis only. Forward analysis with strain estimation provided the most accurate damage-pattern estimation and the highest computational efficiency. Furthermore, the proposed damage identification significantly reduced computation time with the equivalent accuracy compared to the conventional identification procedure, by using damage analysis as the initial estimation.

Keywords: Smart materials; FBG sensor; finite element analysis; stress concentrations; non-destructive testing.

1. INTRODUCTION

Advanced composite materials, such as CFRP, are frequently applied in primary load-bearing structures of newly developed airplanes. Structural health monitoring

Edited by the JSCM.

*To whom correspondence should be addressed. E-mail: yashiro@eng.ehime-u.ac.jp

techniques to evaluate the integrity of such composite structures are quite important for their safety [1]. Fiber Bragg grating (FBG) sensors have suitable characteristics for health monitoring, such as accurate strain and/or temperature measurements, multiplexing capability and embedding capability [2–4]. Strain monitoring has been performed in practical applications of health monitoring by measuring the wavelength shift of the light reflected from the FBG sensor [5]. FBG sensors are also sensitive to local strain changes; these effects appear in the shape of the reflection spectrum [6–8]. Takeda and his colleagues [9, 10] first proposed damage (transverse cracks or delamination) detection in composite laminates using this feature of an FBG sensor.

Complicated damage patterns often appear near stress concentrations in composite laminates [11]. Therefore, health-monitoring techniques should be applied to stress-concentrated sections in real structures. Our previous study [12] demonstrated that the reflection spectrum of an embedded FBG sensor was useful for monitoring damage patterns in notched CFRP laminates, since the spectrum shape contained considerable information on the strain distribution. Moreover, the authors [13] proposed damage identification based on the reflection spectrum as an inverse problem and presented the successful estimation of a damage pattern in a notched laminate.

Some issues, however, still remain in our series of studies. Although we have investigated damage patterns near notches for simplicity, such a configuration may not exist in real structures. More practical stress concentrations must be considered for damage identification. Additionally, the previous damage identification [13] required enormous computational costs, since the tunneling algorithm [14] was introduced to avoid locally optimal solutions of the inverse problem.

This study presents damage identification for a CFRP cross-ply laminate with an open hole using an embedded FBG sensor. It proposes two new approaches to predicting the damage pattern that combine estimation of the applied strain and estimation of the damage pattern with a damage analysis, in order to improve the computational efficiency from the previous damage identification [13]. This study is organized as follows. Section 2 introduces the new procedures for the damage identification. Section 3 describes a tensile test for a holed laminate with an embedded FBG sensor. Section 4 presents the identified results for a numerical example and confirms the proposed approach. Finally, damage identification for the experiment results is demonstrated by four procedures including the previous methods, and accuracy and computational efficiency are discussed.

2. ANALYSIS

2.1. Forward analysis

In order to evaluate the effects of stress concentration and damage on the strain distribution along the embedded FBG sensor, the damage process in a holed

composite laminate was simulated using a layer-wise finite-element model with cohesive elements [12]. Figure 1 illustrates the finite-element mesh considering the

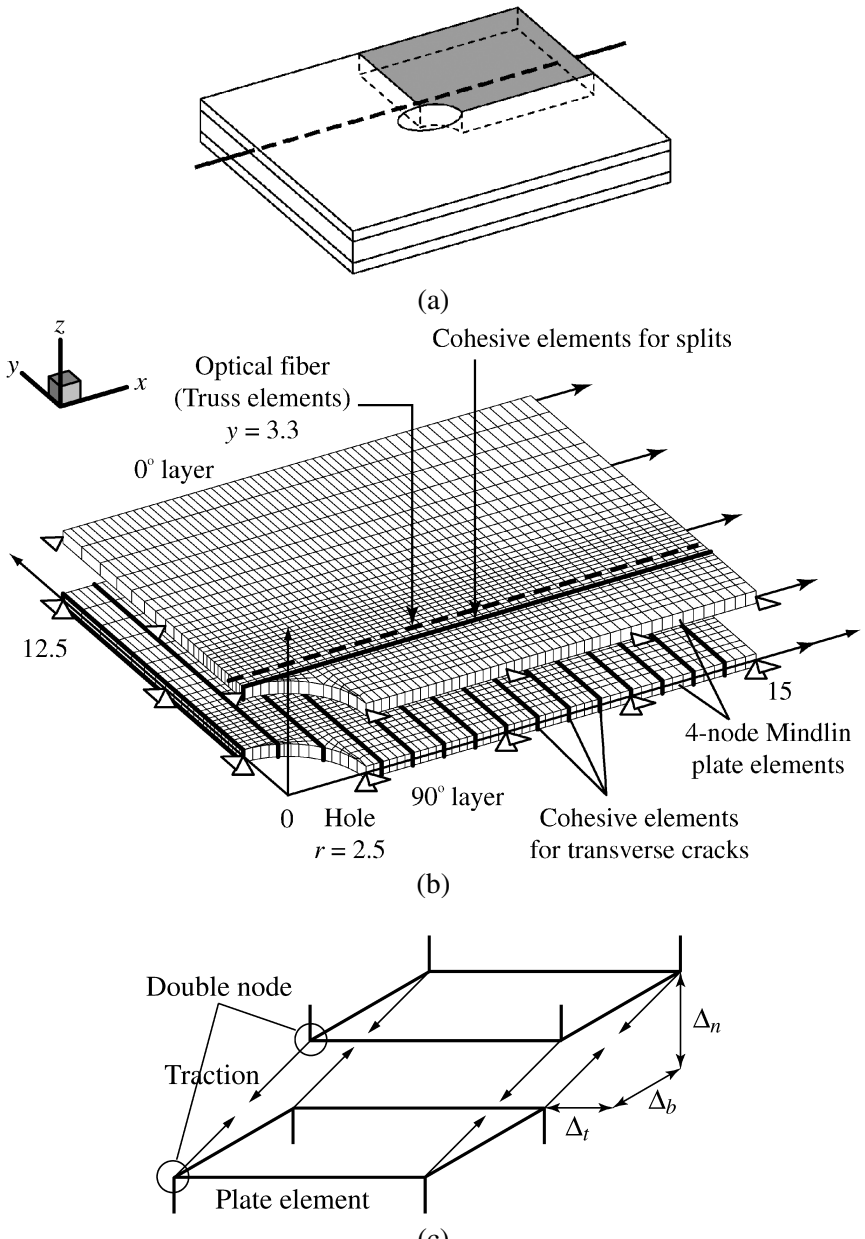

Figure 1. Layer-wise finite-element model of a holed cross-ply laminate with an embedded optical fiber. Cohesive elements for delamination are inserted into all 0°/90° layer interfaces. (a) Schematic. (b) Finite-element mesh. (c) Cohesive element.

symmetry. The dimensions were 15 mm in the longitudinal (x) direction and 12.5 mm in the transverse (y) direction, with a hole radius of 2.5 mm. The model was separated into two layers of 0° and 90° plies to express the stacking configuration of $[0_2/90_2]_s$. Both layers were 0.25 mm thick, and four-node Mindlin plate elements were applied to these layers. An optical fiber was built into the 0° layer with two-node truss elements positioned along the x-direction 0.8 mm from the edge of the hole.

Stress concentration in a cross-ply laminate induces a complicated damage process that concurrently includes splits, transverse cracks and delamination [11]. This damage analysis deals with these types of damage by cohesive elements. Splits in the 0° layer were expressed by four-node cohesive elements located at the hole edge along the x-direction. Four-node cohesive elements for transverse cracks were equally spaced in the x-direction in the 90° layer. Finally, eight-node cohesive elements were inserted into all 0°/90° ply interfaces to express delamination.

As depicted in Fig. 1(c), cohesive elements were assigned to the interfaces between two adjacent plate elements. These cohesive elements act as nonlinear springs that link the plate elements and generate traction resisting the relative displacement between them. The relation between the traction T and the relative displacement Δ is expressed in terms of the residual-strength parameter s [15].

$$T_i = \frac{s}{1-s}\frac{\Delta_i}{\Delta_{ic}}\tau_{i\,\max} \quad (i = n, t, b). \tag{1}$$

Subscripts n, t and b indicate the deformation mode of normal tensile cracking (mode I), in-plane shear cracking (mode II), and out-of-plane shear cracking (mode III). $\tau_{i\,\max}$ and Δ_{ic} $(i = n, t, b)$ are the strength and the critical relative displacement in each cracking mode. The critical relative displacements are defined by the following expression:

$$\Delta_{nc} = \frac{2G_{\mathrm{Ic}}}{\tau_{n\,\max} s_{\mathrm{ini}}}, \quad \Delta_{tc} = \frac{2G_{\mathrm{IIc}}}{\tau_{t\,\max} s_{\mathrm{ini}}}, \quad \Delta_{bc} = \frac{2G_{\mathrm{IIIc}}}{\tau_{b\,\max} s_{\mathrm{ini}}}, \tag{2}$$

where G_{ic} $(i = n, t, b)$ is the critical energy-release rate, and s_{ini} (=0.999) is the initial value of the residual-strength parameter. The residual-strength parameter is defined as a function of the normalized relative-displacement vector $\tilde{\boldsymbol{\Delta}} = \{\Delta_n/\Delta_{nc}, \Delta_t/\Delta_{tc}, \Delta_b/\Delta_{bc}\}^{\mathrm{T}}$.

$$s = \min\left[s_{\min}, \max[0, 1 - |\,\tilde{\boldsymbol{\Delta}}\,|]\right]. \tag{3}$$

The value of s decreases as the relative displacements between two adjacent plate elements become larger, and a cohesive element generates a crack surface that yields no traction if $s = 0$.

We simulated the damage extension and obtained the strain distribution of the optical fiber by applying uniform tensile displacements to the end of the model ($x = 15$ mm). Thermal residual stresses for the temperature change ($\Delta T = -165$ K) were also considered.

An FBG sensor has periodic changes in the refractive index of the core in the optical fiber. A narrow-band component is then reflected following injection of broadband light, and its wavelength or the reflection spectrum is influenced by the distribution of the grating period Λ and the effective refractive index of the core n_{eff}. These sensor parameters depend on the longitudinal strain $\varepsilon_f(x)$, while x denotes the longitudinal direction of the optical fiber [16]:

$$\Lambda(x) = \big(1 + \varepsilon_f(x)\big)\Lambda_{\text{ini}}, \tag{4}$$

$$n_{\text{eff}}(x) = n_0 + \Delta n(x) = n_0 - \frac{n_0^3}{2}\{p_{12} - \nu_f(p_{11} + p_{12})\}\varepsilon_f(x). \tag{5}$$

Λ_{ini} is the initial grating period, n_0 is the initial refractive index of the core, ν_f is Poisson's ratio of the glass, and p_{11} and p_{12} denote Pockel's constants where indices 1 and 2 indicate the longitudinal and transverse direction of the optical fiber. The transfer-matrix method [17] can numerically calculate a reflection spectrum that contains the effect of the damage in the holed specimen, by substituting the strain distribution of the optical fiber obtained in the above damage analysis into equations (4) and (5) and using these sensor profiles. The gage length of the FBG sensor was 10 mm, and an end of the gage section was positioned at $(x, y) = (0, 3.3)$ in the finite-element model.

2.2. Estimation of the applied strain

The highest reflectivity is obtained at the following wavelength in an FBG sensor [2, 3]:

$$\lambda = 2n_{\text{eff}}\Lambda. \tag{6}$$

Equations (4) and (5) imply that the peak wavelength λ is a function of the longitudinal strain along the FBG sensor. Accordingly, the applied strain that corresponds to the input (experimental) spectrum can be obtained by matching the peak wavelength of the estimation to the input.

We therefore estimated the applied strain ε_{a} by searching for the following condition:

$$F_1(\varepsilon_{\text{a}}) = \lambda_0 - \tilde{\lambda} = 0. \tag{7}$$

λ_0 and $\tilde{\lambda}$ are the peak wavelengths for the input spectrum and the estimated spectrum, where the peak wavelength is defined as the center wavelength at a quarter reflectivity in the deformed spectrum. The Newton–Raphson method was utilized in this procedure.

2.3. Estimation of the damage pattern

The shape of the reflection spectrum from the embedded FBG sensor was used in estimating the damage pattern near the hole. Estimation of the damage pattern can be defined as an optimization problem that minimizes the square errors between the

input (experimental) spectrum and the temporarily estimated spectrum as a function of some variables **d** to represent a damage pattern near the hole.

$$\text{Minimize: } F_2(\mathbf{d}) = \sum_{m=0}^{100} \{a_m - \tilde{a}_m(\mathbf{d})\}^2$$
$$\text{Design variables: } \mathbf{d} = \{d_{\mathrm{d}1}, d_{\mathrm{d}2}, d_{\mathrm{d}3}, \alpha, \beta, p, d_{\mathrm{c}}\}^{\mathrm{T}}. \tag{8}$$

The reflection spectra were expressed by a Fourier series under the 100-th order to quantitatively evaluate their shapes. Here, a_m and $\tilde{a}_m$ are the m-th Fourier coefficients for the input and estimated spectrum shapes. Design variables **d** that minimize square errors $F_2(\mathbf{d})$ are considered to be the identified results.

In the damage analysis, the residual-strength parameter s defines the stiffness in each cohesive element, and the distribution of the parameter s of all cohesive elements can then approximate a damage pattern in the laminate. The reflection spectrum $\tilde{a}_m$ is optimized by utilizing the change in the strain distribution that results from the changes in the stiffness for all cohesive elements as a function of design variables **d**.

Figure 2 defines the design variables **d** to represent the damage pattern or the distribution of the parameter s. The variables $d_{\mathrm{d}1}$ and $d_{\mathrm{d}2}$ express the size of the delamination, and α and β define the shape of the delaminated area. The residual-strength parameter $s = 0$ is given for each cohesive element in the delamination. The delamination process zone (the region where $0 < s < s_{\mathrm{ini}}$) is also considered, and its size is expressed by the variable $d_{\mathrm{d}3}$. The value s in the process zone is distributed by the variable p that governs the recovery of the residual strength. The distance from the hole edge to the transverse crack farthest from the hole is defined as the design variable d_{c}. The embedding of an FBG sensor in this study offers little sensitivity to the splits [12]. The lengths of the split $d_{\mathrm{s}1}$ and the splitting process zone $d_{\mathrm{s}2}$ are then related to the delamination process zone $d_{\mathrm{d}3}$, since the delamination extends along splits [11]. We assume that the tip of the split coincides with that of the delamination process zone, as illustrated in Fig. 2(a) and (c). A small splitting process zone (1 mm) is also assumed. The value of the residual-strength parameter s in the splitting process zone is distributed by the variable p as in the delamination process zone.

A finite-element analysis with the determined distribution of the residual-strength parameter provides the strain distribution of the FBG sensor at the damage pattern **d**. The following optical analysis can simulate the corresponding reflection spectrum $\tilde{a}_m(\mathbf{d})$ that includes the effects of the damage as well as the stress concentration due to the hole. We applied mathematical programming (Fletcher–Powell method with the golden-section linear search) to equation (8) and optimized the damage pattern **d**.

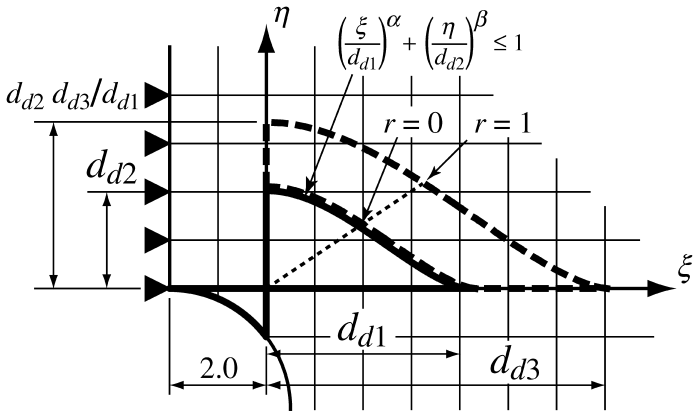

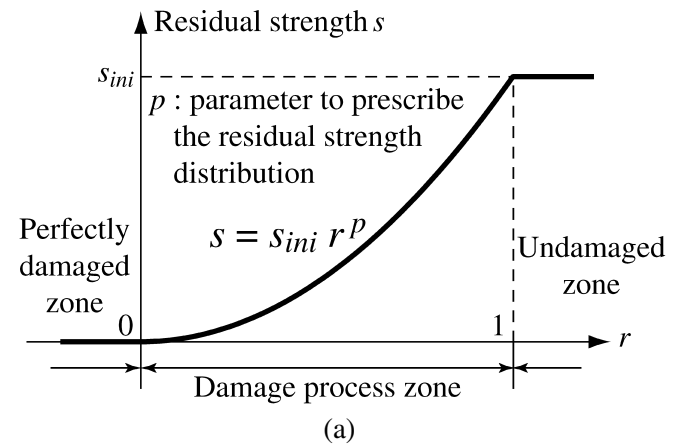

(a)

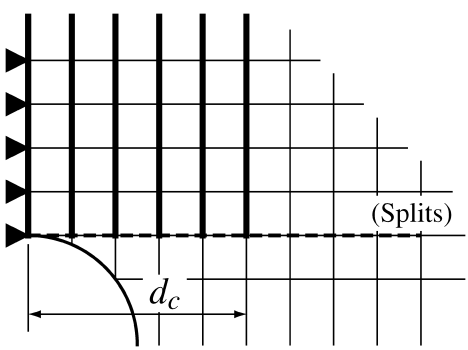

(b)

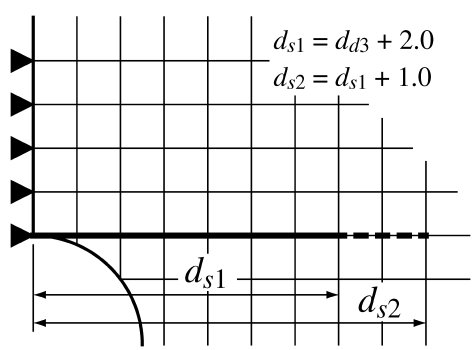

(c)

Figure 2. Definition of the design variables representing the damage pattern near the hole. (a) Delamination (━━ perfectly damaged zone; ▬ ▬ damaged process zone). (b) Transverse cracks. (c) Splits.

2.4. Analytical procedure

This study proposes two new approaches to predicting the damage pattern. One is a combination of forward analysis and the estimation of the applied strain. The other is the estimation of the damage pattern combined with the damage analysis and the estimation of the applied strain (termed damage identification).

Figure 3 illustrates the flowcharts of the two approaches. Forward analysis with strain estimation continuously performs the forward analysis at the estimated applied strain until the peak wavelength of the simulated spectrum coincides with the one of the input, as indicated in Fig. 3(a).

In the damage identification (Fig. 3(b)), the damage pattern is first obtained by the damage analysis at the applied strain calculated from the input spectrum by equation (6). We use the distribution of the residual-strength parameter s as the initial estimation for the design variables $\mathbf{d}$ and obtain these values as follows.

Size of the delamination:

(1) d_{d1}: The maximum value along the x-coordinate in the completely damaged delamination where the parameter $s = 0$.

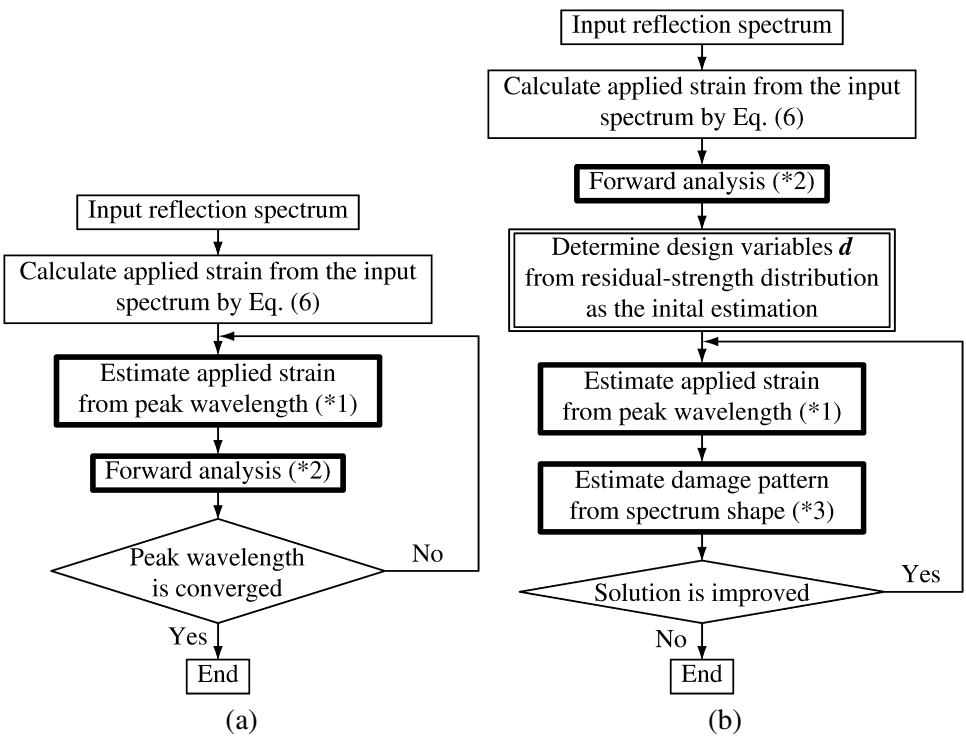

Figure 3. Flowchart of (a) forward analysis with the strain estimation and (b) damage identification. (*1) Search $F_1(\varepsilon_{\mathrm{a}}) = 0$, while damage state of the cohesive elements is kept constant. (*2) The damage analysis and the optical analysis. (*3) Minimize $F_2(\mathbf{d})$, while applied strain is kept constant.

(2) d_{d2}: The maximum value along the y-coordinate in the completely damaged delamination.

(3) d_{d3}: The maximum value along the x-coordinate in the delamination process zone.

Shape of the delamination:

(1) Set β to 1.0.

(2) Find the intersecting position of the delamination tip and the FBG sensor.

(3) Search for the value of α that approximates the delamination passing the above indicated position as well as the other two points $(x, y) = (2.0, d_{d2})$ and $(d_{d1}, 2.5)$.

The variable p for the delamination process zone: Assumed to be 1.0.

Transverse cracks d_c: The maximum value along the x-axis of completely damaged cohesive elements.

Estimation of applied strain and damage-pattern estimation are then alternately iterated as long as the value of $F_2(\mathbf{d})$ becomes smaller.

The proposed damage identification utilizes the results of the damage analysis as the reliable estimation. Although the objective function $F_2(\mathbf{d})$ contains many locally optimal solutions, this step enables us to avoid inappropriate solutions without the tunneling algorithm [14], which was introduced in the previous study [13].

3. EXPERIMENTAL

3.1. Materials

A CFRP cross-ply laminate (T800H/3631, Toray Industries, Inc.) was used with a stacking configuration of $[0_2/90_2]_s$. Figure 4 depicts the dimensions of a specimen.

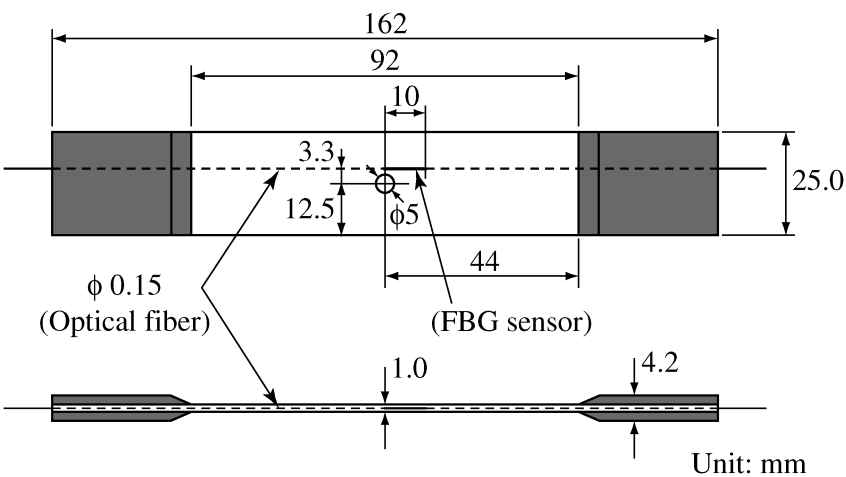

Figure 4. Dimensions of the specimen with an embedded FBG sensor. The stacking configuration was cross-ply $[0_2/90_2]_s$. The FBG sensor was embedded in a 0° ply at the 0°/90° ply interface.

The specimen coupon was holed at the center. The hole diameter was 5 mm, while the specimen width was 25 mm. An optical fiber with an FBG sensor (NTT Advanced Technology Corporation) was embedded in a 0° ply along the fiber direction at the 0°/90° ply interface. The gage length of the FBG sensor was 10 mm, and its end was located nearest to the hole edge.

A quasi-static tensile test was conducted for the holed specimen at room temperature. The specimen was loaded using a universal electromechanical testing system (Instron 5582, Instron Corp.) at a cross-head speed of 0.25 mm/min. The applied strain was measured by an extensometer with a gage length of 50 mm, and the tensile load was simultaneously obtained by a load cell. Broadband light was injected into the optical fiber by a light source (AQ4310(155), Ando Electric Co., Ltd.) through a circulator. The spectrum of the reflected light from the FBG sensor was measured using an optical spectrum analyzer (AQ6317, Ando Electric Co., Ltd.). The reflection spectra were measured at several applied strains while the load was held constant. The specimen was then unloaded to observe the damage using soft X-ray radiography.

3.2. Experimental results

Figures 5(a-1), (b-1) and (c-1) illustrate the typical damage progress observed by soft X-ray radiography. Splits in 0° plies and transverse cracks in 90° plies first appeared at the edge of the hole. The splits extended along the fiber direction, and the number of transverse cracks increased as the load increased. Delamination at the 0°/90° ply interface then extended in a quarter-elliptical shape along the splits.

The corresponding reflection spectra of the FBG sensor are plotted in Figs 6(a-1), (b-1) and (c-1). The spectrum shifted toward a longer wavelength and became broad with increased loading. The spectrum exhibited some peaks when transverse cracks were generated, as depicted in Fig. 6(a-1). Two large peaks appeared in the spectrum when the delamination was initiated, and the peak at the longer wavelength became larger with increasing delamination, as represented in Figs 6(b-1) and (c-1). Thus, the overall spectrum shape was significantly deformed by the damage extension.

4. RESULTS AND DISCUSSION

4.1. Damage identification for a numerical example

We applied the proposed damage identification described in Fig. 3(b) to the simulated results at 0.8% applied strain. Material properties and parameters for cohesive elements are listed in Table 1; optical properties for the FBG sensor are listed in Table 2. Here, the critical energy-release rates for the cohesive elements were determined by fitting the damage patterns obtained in the damage analysis to the experiments.

Figure 7 depicts the estimated results. The estimated reflection spectrum almost coincided with the input spectrum that has a broad shape and a large peak at

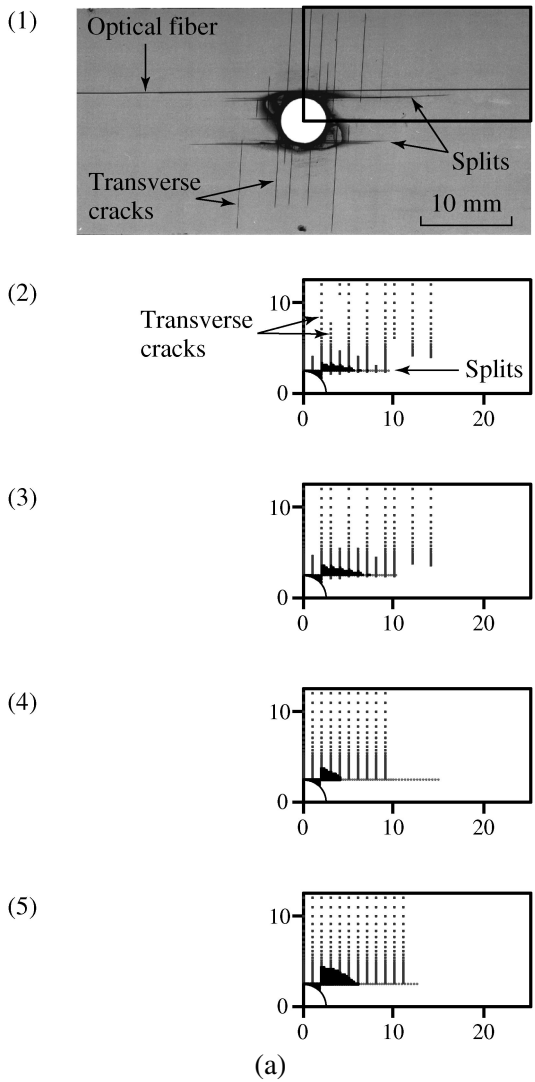

Figure 5. Damage patterns of the holed cross-ply laminate: (1) experiment; (2) forward analysis; (3) forward analysis with the strain estimation; (4) damage identification; and (5) previous damage identification. Each dot represents a completely damaged cohesive element. (a) 0.68% strain.

1568 nm. The applied strain was estimated at 0.8% and was identical with that in the simulation. The estimated damage pattern also agreed well with the simulated one that has splits, transverse cracks and delamination along the splits.

Figure 7(c) plots the longitudinal strain distribution of the embedded FBG sensor. Local strain changes due to transverse cracks were visible in $0 < x < 2$ mm and $x > 9$ mm. Almost constant strain in the range $2 < x < 5$ mm corresponded to the delamination. In general, constant strain and local strain changes appear in

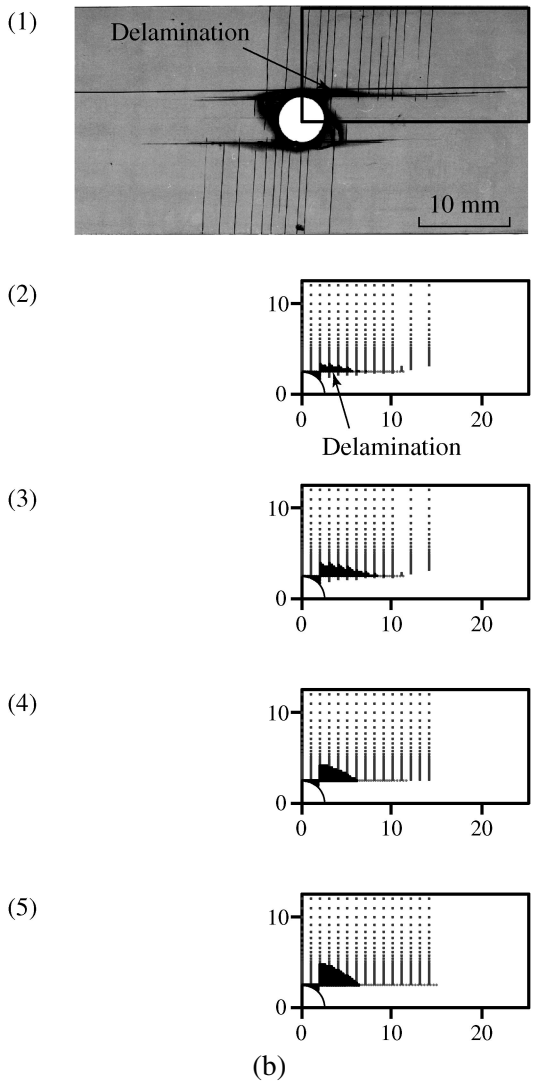

Figure 5. (b) 0.83% strain.

a reflection spectrum as a large peak and small changes in reflectivity [12]. The proposed damage identification thus utilizes the information on the longitudinal strain distribution of the FBG sensor contained in the reflection spectrum.

4.2. Damage identification for the experiment results

We predicted the damage patterns observed in the experiment using the proposed approaches. The forward analysis only and the conventional damage identification

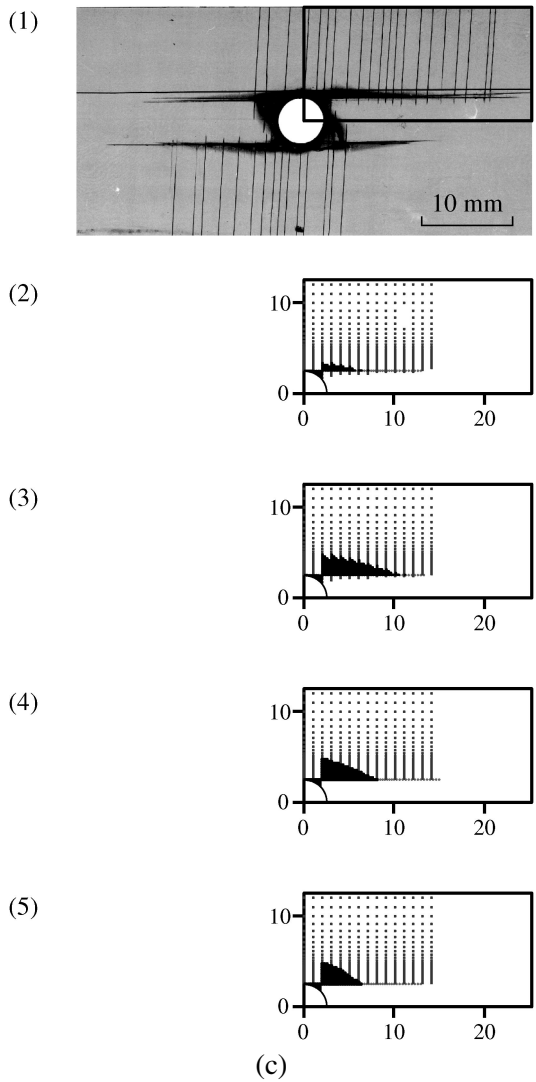

Figure 5. (c) 1.00% strain.

[13] were also carried out for comparison. Figures 5 and 6 illustrate the obtained damage patterns and the reflection spectra along with the experiment results.

The predicted peak wavelength differed from the experimental one as illustrated in Fig. 6(a-2) when the applied strain measured by the extensometer was used in the forward analysis. In contrast, the forward analysis with the strain estimation provided the peak wavelength that was identical to the experiment, as depicted in Fig. 6(a-3). In this case, the damage extension and the reflection spectra were similar to the experiment results, as depicted in Figs 5(a-3)–(c-3) and Figs 6(a-3)–(c-3).

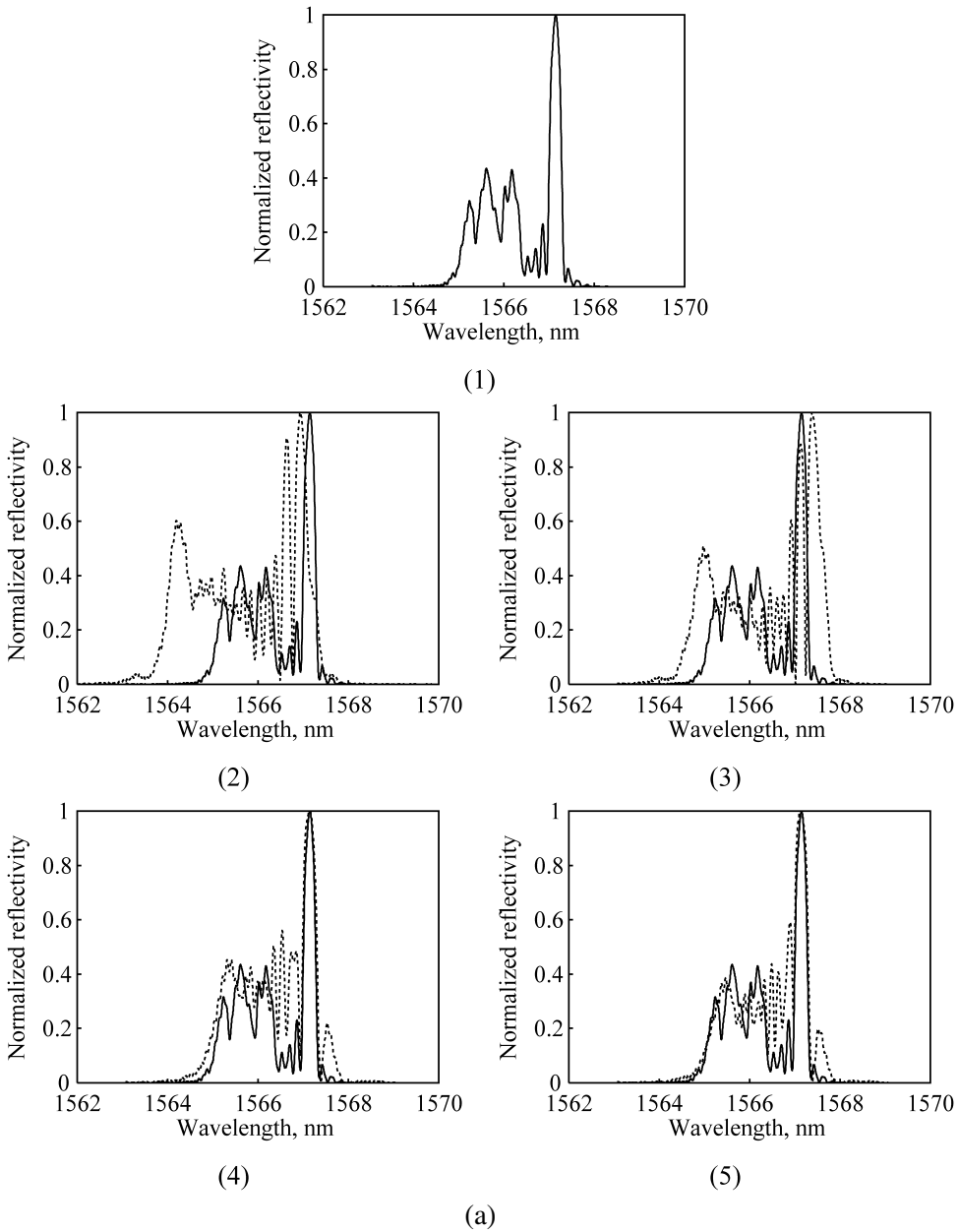

Figure 6. Reflection spectra of the embedded FBG sensor: (1) experiment; (2) forward analysis; (3) forward analysis with the strain estimation; (4) damage identification; and (5) previous damage identification. Solid lines are the measured spectra. (a) 0.68% strain.

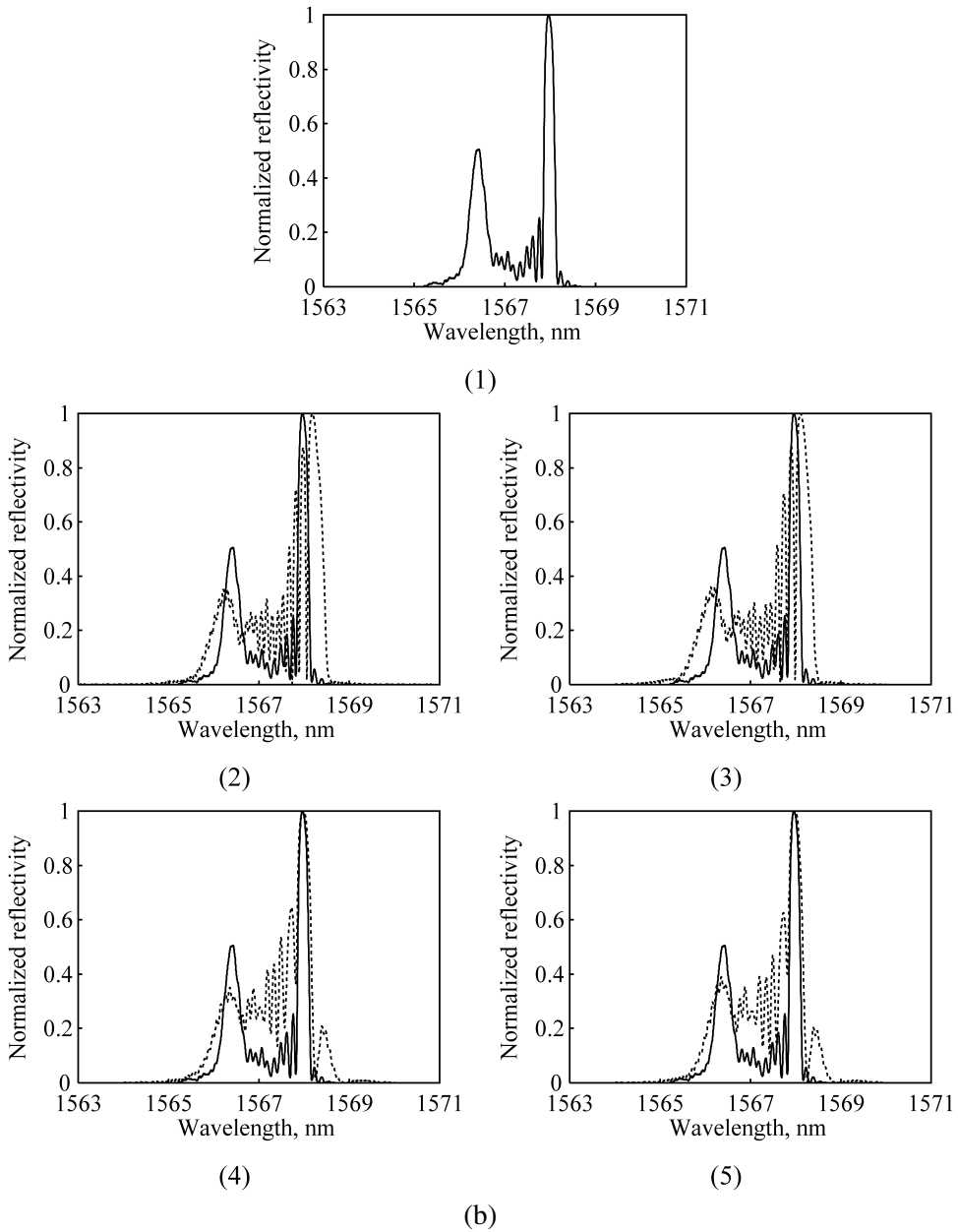

Figure 6. (b) 0.83% strain.

The proposed damage identification produced reflection spectra that agreed well with the experimental ones, as illustrated in Figs 6(a-4)–(c-4). Figures 5(a-4) to (c-4) are the corresponding damage patterns where splits and transverse cracks are well estimated. However, the delamination size was overestimated in the transverse

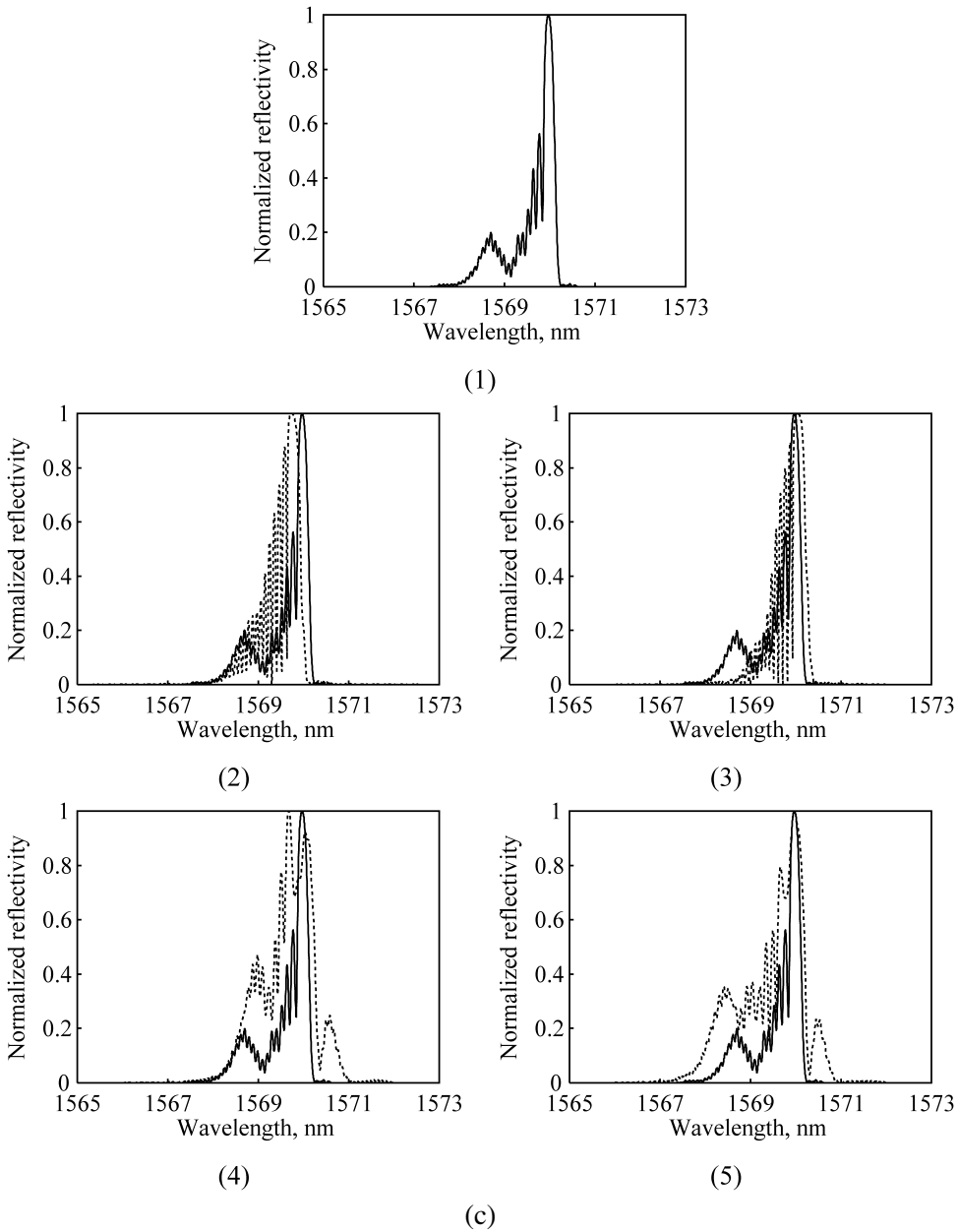

Figure 6. (c) 1.00% strain.

direction. This overestimation may result from the low sensitivity of an FBG sensor to strain in the direction normal to itself. The damage-pattern estimation will be improved by using additional FBG sensors embedded in the transverse position of the specimen. We also verified that the proposed approach could offer almost

Table 1.
Material properties used in the analysis

(a) Materials	
CFRP T800H/3631	
Longitudinal Young's modulus (GPa)	148
Transverse Young's modulus (GPa)	9.57
In-plane shear modulus (GPa)	4.50
Out-of-plane shear modulus (GPa)	3.5
In-plane Poisson's ratio	0.356
Out-of-plane Poisson's ratio	0.49
Longitudinal thermal expansion coefficient ($\times 10^6$/K)	-0.6
Transverse thermal expansion coefficient ($\times 10^6$/K)	36.0
Optical fiber	
Young's modulus of glass (GPa)	73.1
Young's modulus of coating (GPa)	1.47
Thermal expansion coefficient of glass ($\times 10^6$/K)	0.5
Thermal expansion coefficient of coating ($\times 10^6$/K)	60
(b) Cohesive elements	
For splits and transverse cracks	
In-plane tensile strength (MPa)	83.7
In-plane shear strength (MPa)	100
Out-of-plane shear strength (MPa)	100
Mode I critical energy release rate (J/m^2)	310
Mode II critical energy release rate (J/m^2)	600
Mode III critical energy release rate (J/m^2)	600
For delamination	
In-plane tensile strength (MPa)	40
In-plane shear strength (MPa)	60
Out-of-plane shear strength (MPa)	60
Mode I critical energy release rate (J/m^2)	500
Mode II critical energy release rate (J/m^2)	700
Mode III critical energy release rate (J/m^2)	700

Table 2.
Parameters of the optical fiber and the FBG sensor

Gage length (mm)	10
Initial center wavelength λ (nm)	1556.2
Initial refractive index of the core n_0	1.4490
Poisson's ratio of the glass ν_f	0.16
Strain-optic coefficients p_{11}	0.113
Strain-optic coefficients p_{12}	0.252

identical results to the conventional damage identification depicted in Figs 5(a-5) to (c-5) and Figs 6(a-5) to (c-5).

Table 3 lists the computation time for each approach. A personal computer (Pentium 4 – 3.2 GHz with 2 GB memory) was used in all calculations. The forward analysis only and the forward analysis with the strain estimation needed

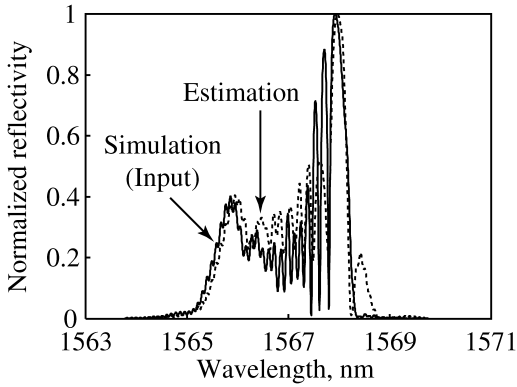

(a)

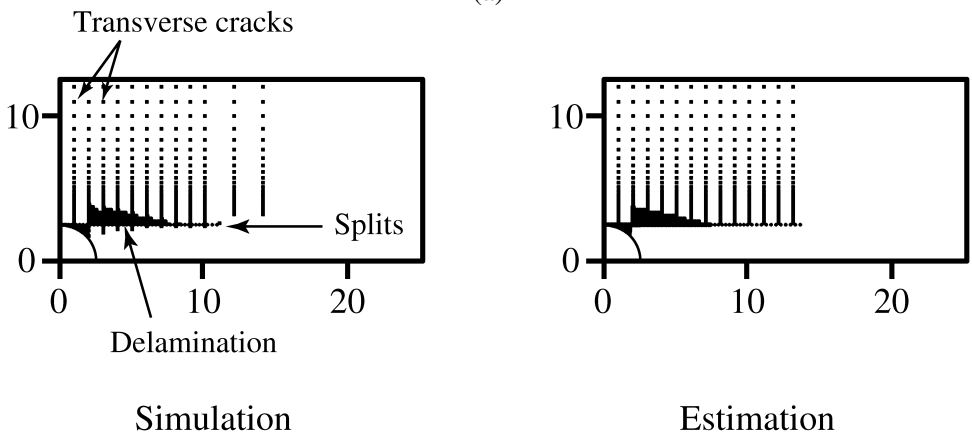

(b)

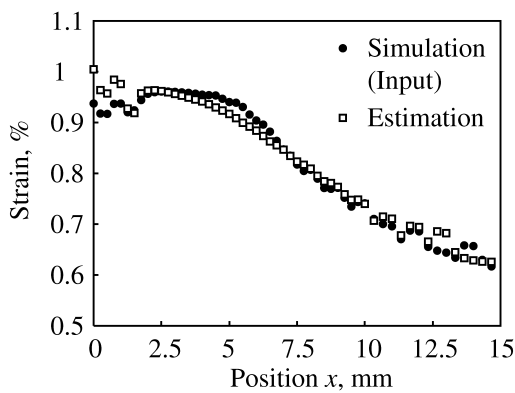

(c)

Figure 7. Identified results for a numerical example. (a) Reflection spectrum. (b) Damage pattern. (c) Strain distribution.

Table 3.
Computation time (in seconds) required for predicting and identifying the damage pattern

	(1)	(2)	(3)	(4)
(a) 0.68%	7.67×10^2	1.65×10^3	5.72×10^3	2.35×10^5
(b) 0.83%	1.21×10^3	2.64×10^3	6.98×10^3	8.44×10^5
(c) 1.00%	6.45×10^2	1.06×10^3	2.51×10^3	2.35×10^5

(1) Forward analysis. (2) Forward analysis with strain estimation. (3) Damage identification. (4) Damage identification with tunneling algorithm.

less time than the others at all applied strains. Therefore, we concluded that the forward analysis with the strain estimation could provide the best prediction from the viewpoints of accuracy and efficiency. It should be noticed that the results of the forward analysis depend heavily on the parameters for the cohesive elements. The damage identification may provide better estimation than the forward analysis with the strain estimation, unless these parameters are determined. We also found that the proposed damage identification significantly reduced computation time with the equivalent accuracy compared to the conventional procedure.

5. CONCLUSIONS

This study presented the identification of the damage patterns in a holed CFRP cross-ply laminate using the reflection spectrum from an embedded FBG sensor. It proposed two new approaches that combine estimation of the applied strain and estimation of the damage pattern with damage analysis, in order to improve the computational efficiency from our previous procedure. The conclusions are summarized below.

(1) We experimentally confirmed that the shape of the reflection spectrum from the embedded FBG sensor was considerably deformed as the damage near the hole, i.e. splits, transverse cracks and delamination, extended.

(2) We demonstrated that the proposed damage identification accurately estimated the damage pattern for the numerical example.

(3) We predicted the damage patterns observed in the experiment using the proposed approaches as well as the forward analysis only and conventional damage identification. The forward analysis with strain estimation offered the best prediction from the viewpoints of accuracy and computation efficiency.

(4) The proposed damage identification significantly reduced computation time with equivalent accuracy compared to the previous procedure.

REFERENCES

1. F. K. Chang (Ed.), *Structural Health Monitoring 2003*. DESTechnol Publications, Lancaster (2003).

2. K. O. Hill and G. Meltz, Fiber Bragg grating technology fundamentals and overview, *J. Lightwave Technol*. **15**, 1263–1276 (1997).
3. A. D. Kersey, M. A. Davis, H. J. Patrick, M. LeBlanc, K. P. Koo, C. G. Askins, M. A. Putnam and E. J. Friebele, Fiber grating sensors, *J. Lightwave Technol*. **15**, 1442–1463 (1997).
4. C. I. Merzbacher, A. D. Kersey and E. J. Friebele, Fiber optic sensors in concrete structures: a review, *Smart Mater. Struct*. **5**, 196–208 (1996).
5. A. D. Kersey, M. A. Davis, T. A. Berkoff, D. G. Bellemore, K. P. Koo and R. T. Jones, Progress towards the development of practical fiber Bragg grating instrumentation systems, in: *Proc. SPIE* **2839**, 40–63. SPIE, Denver, CO (1996).
6. P. C. Hill and B. J. Eggleton, Strain gradient chirp of fiber Bragg gratings, *Electron. Lett.* **30**, 1172–1174 (1994).
7. M. LeBlanc, S. Y. Huang, M. M. Ohn and R. M. Measures, Tunable chirping of a fiber Bragg grating using a tapered cantilever bed, *Electron. Lett.* **30**, 2163–2165 (1994).
8. K. Peters, M. Studer, J. Botsis, A. Iocco, H. Limberger and R. Salathe, Embedded optical fiber Bragg grating sensor in a nonuniform strain field: measurements and simulations, *Exp. Mech.* **41**, 19–28 (2001).
9. Y. Okabe, S. Yashiro, T. Kosaka and N. Takeda, Detection of transverse cracks in CFRP composites using embedded fiber Bragg grating sensors, *Smart Mater. Struct*. **9**, 832–838 (2000).
10. S. Takeda, Y. Okabe and N. Takeda, Delamination detection in CFRP laminates with embedded small-diameter fiber Bragg grating sensors, *Composites Part A* **33**, 971–980 (2002).
11. M. T. Kortschot and P. W. R. Beaumont, Damage mechanics of composite materials: I – Measurements of damage and strength, *Compos. Sci. Technol*. **39**, 289–301 (1990).
12. S. Yashiro, N. Takeda, T. Okabe and H. Sekine, A new approach to predicting multiple damage states in composite laminates with embedded FBG sensors, *Compos. Sci. Technol*. **65**, 659–667 (2005).
13. N. Takeda, S. Yashiro and T. Okabe, Estimation of the damage patterns in notched laminates with embedded FBG sensors, *Compos. Sci. Technol.* **66**, 684–693 (2006).
14. A. V. Levy and A. Montalvo, The tunneling algorithm for the global minimization of functions, *SIAM J. Sci. Comput*. **6**, 15–29 (1985).
15. P. H. Geubelle and J. S. Baylor, Impact-induced delamination of composites: a 2D simulation, *Composites Part B* **29**, 589–602 (1998).
16. R. J. Van Steenkiste and G. S. Springer, *Strain and Temperature Measurement with Fiber Optic Sensors*. Technomic Publications, Lancaster (1997).
17. S. Huang, M. LeBlanc, M. M. Ohn and R. M. Measures, Bragg intragrating structural sensing, *Appl. Opt.* **34**, 5003–5009 (1995).